Theoretical study of the low-lying excited singlet states of furan

E. V. Gromov, A. B. Trofimov, and N. M. Vitkovskaya
Laboratory of Quantum Chemistry, Computer Center, Irkutsk State University, 664003 Irkutsk, Russian Federation

J. Schirmer and H. Köppel
Theoretische Chemie, Physikalisch-Chemisches Institut, Universität Heidelberg, Im Neuenheimer Feld 229, D-69120 Heidelberg, Germany

(Received 4 February 2003; accepted 7 April 2003)

The lowest two Rydberg and two $\pi-\pi^*$ valence excited singlet states of furan [referred to as $^1A_2(3s)$, $^1B_1(3p)$ and $^1B_2(V)$, $^1A_1(V')$, respectively, at the C_{2v} ground-state molecular configuration] have been studied using the equation-of-motion coupled-cluster singles and doubles method (EOM-CCSD). Full geometry optimizations with subsequent computation of harmonic vibrational frequencies have been performed in order to locate and characterize stationary points on the potential energy surfaces (PES). The latter optimization work was enabled by the availability of analytic energy gradient techniques for the EOM-CCSD approach. A major new finding is that both the $^1B_2(V)$ and $^1A_1(V')$ valence states are unstable with respect to non-totally symmetric distortions at the C_{2v} configuration. The symmetry breaking in the $^1B_2(V)$ state involves an in-plane coordinate of b_2 symmetry. The relaxation process begins on the S_2 adiabatic PES and, after passing through a conical intersection of the S_2 and S_1 PES, continues on the S_1 surface, taking the system finally to the adiabatic minimum of S_1 ($^1A_2$ state). The $^1A_1(V')$ valence state is found to be unstable with respect to the out-of-plane bending coordinates of b_1 and a_2 symmetry. The resulting relaxed molecular structures have C_s and C_2 symmetry, respectively. The present findings are analyzed in terms of a linear vibronic coupling model and spectroscopic implications are discussed. © *2003 American Institute of Physics.* [DOI: 10.1063/1.1578051]

I. INTRODUCTION

The furan molecule (Fig. 1) belongs to the basic heteroaromatic compounds relevant for many fields of modern chemistry, ranging from the study of natural products and biologically active substances to the development of building-blocks for organic synthesis and conducting polymers.[1] The contemporary knowledge of the electronic spectra and structure of furan has been gathered in many experimental[2–17] and theoretical[3,18–27] studies. The ongoing interest in the excited states of furan is reflected by several recent publications.[2,18–20] At the same time, some important aspects of the subject are still poorly understood. A prominent example here is the first absorption band in the VUV spectrum of furan, located in the energy region 5.7–6.5 eV.[3] The band is strikingly diffuse and has scarce irregular vibronic structure, which hardly allows for any definitive assignment. Though at present all excited states of furan, contributing to that part of the spectrum are firmly established, and their excitation energies are known to a good accuracy, a consistent theoretical interpretation of the observed spectral envelope is still not available. Even less is known of the nuclear dynamics following the electronic excitation, the possible energy redistribution and relaxation mechanisms.

The complex pattern of the furan VUV spectrum suggests a vibronic nature of the underlying excited states and the presence of nonadiabatic effects. As now is well recognized, such effects are very common and often become important for spectroscopy, internal energy redistribution and collision processes.[28–33] According to our earlier work,[23] vibronic coupling effects in furan are to be expected already for the lowest excited singlet states associated with the first VUV absorption maximum. The most important of these states are: $^1A_2(3s)$, $^1B_2(V)$, $^1B_1(3p)$, and $^1A_1(V')$. As indicated by the notation, the $^1A_2$ and $^1B_1$ states have Rydberg character, whereas the $^1B_2$ and $^1A_1$ states are $\pi-\pi^*$ valence-type excitations (Fig. 1). Vibronic interaction among these states is likely to occur, since the states lie (vertically) within a narrow energy region of about 0.7 eV, and the molecule possesses sufficient vibrational modes in each symmetry species, making possible all kinds of couplings (8 a_1-modes, 3 a_2-modes, 3 b_1-modes, and 7 b_2-modes). According to our experience in the furan cation (and other five-membered heterocyclic molecular ions),[34] we should expect the presence of many medium strong couplings, building up a substantial cumulative effect.

The actual vibronic coupling mechanisms can, of course, be established only from an analysis of the potential energy surfaces (PES) for the interacting states. The typical signatures of vibronic interaction are conical intersections of the PES (Refs. 28, 35, and 36) and nontotally symmetric distortions of the excited molecules (symmetry breaking).[32,33] For furan no such analysis of the excited-state PES properties has been done so far, and there are only three previous studies, in which the excited states have been treated beyond the vertical electron excitation picture.[18,21,23]

In our previous ADC(2) (second-order algebraic-diagrammatic construction) polarization propagator study of

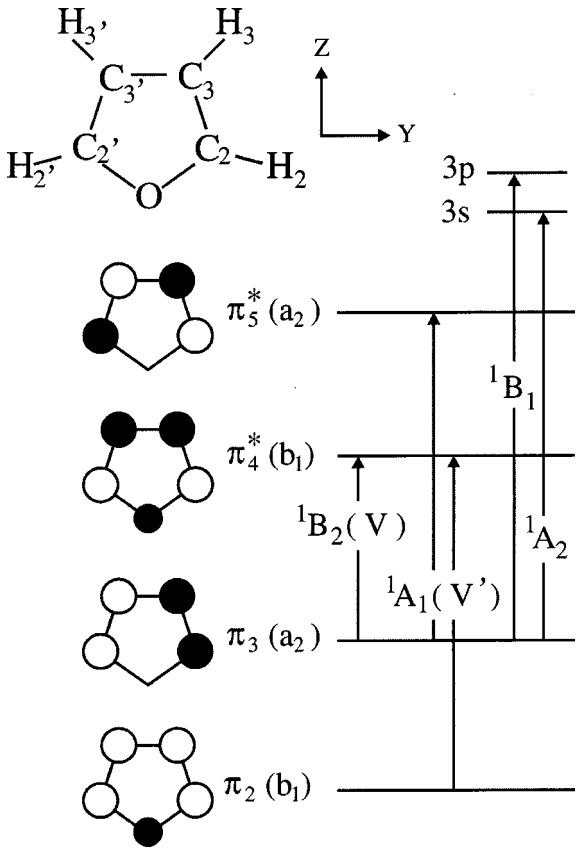

FIG. 1. Geometry, π orbitals, and possible low-lying valence and Rydberg transitions of furan.

electron excitations in furan we have estimated adiabatic transition energies using a linear vibronic coupling (LVC) model, which accounts for structural relaxations along totally symmetric modes.[23] Another study of adiabatic transition energies in furan was performed by Christiansen and Jørgensen[21] using the linear response (LR) coupled-cluster (CC) approach. In their work, excited-state geometries were optimized using numeric gradients at the CC2 approximation level.[37] An interesting finding of this work is a structural instability of the $^1A_1(V')$ valence state, leading to a C_s configuration of the molecule. Transitions to the other low-lying singlet states, including the $^1B_2(V)$ valence states, were predicted to maintain the original C_{2v} symmetry. Recently, Burcl *et al.*[18] performed a geometry optimization and harmonic frequency analysis for the $^1A_2(3s)$, $^1B_2(V)$, and $^1B_1(3p)$ excited states of furan using time-dependent density-functional theory (DFT). In contrast to the results of Christiansen and Jørgensen,[21] an out-of-plane bent equilibrium configuration was predicted for the $^1B_2(V)$ valence state. No geometry optimization results were reported for the $^1A_1(V')$ valence state.

As a basic step towards the understanding of vibronic effects in the excited furan molecule, we study in the present work the PES of the four low-lying excited singlet states [referred to as $^1A_2(3s)$, $^1B_1(3p)$, $^1B_2(V)$, and $^1A_1(V')$ at the C_{2v} ground-state molecular configuration]. To ensure a reliable description of the electronic structure, we use the equation-of-motion coupled-cluster singles and doubles (EOM-CCSD) approach.[38] The EOM-CCSD method, which is (as far as the excitation energies are concerned) fully equivalent to the symmetry adapted cluster (SAC-CI) method[39] and coupled cluster linear response (CCLR) theory,[40] is well suited to the objectives of our study, since it combines high accuracy with acceptable computational costs, allowing us to use fairly large basis set. Another advantage of the EOM-CCSD approach for the present study is the availability of analytic energy gradients,[41] making feasible a full geometry optimization for the excited states and the calculation of harmonic vibrational frequencies at the stationary points. Finally, one should mention the size-consistency property of the CC approach and the possibility to use it as a blackbox method.

In the present work we focus on the structural aspects of the vibronic interaction in excited furan. The development of suitable vibronic models and their use in actual dynamical calculations will be deferred to a forthcoming communication.[42]

II. COMPUTATIONAL PROCEDURES

The full geometry optimization for excited states of furan was performed using the EOM-CCSD method with analytic energy gradients,[38,41] as implemented in the ACES II *ab initio* program package.[43] For each stationary point harmonic vibrational frequencies and zero-point vibrational energies (ZPVE) were computed. The type of the stationary point was established using the eigenvalues and eigenvectors of the Hessian matrix. The second energy derivatives with respect to the nuclear coordinates were evaluated by numeric differentiation of the analytic gradients. The calculations for the electronic ground state were done using the conventional CCSD approach.[44]

For calculating vertical excitation energies we also used the (internally-contracted) multi-reference configuration interaction (MRCI) method,[45] based on molecular orbitals (MO) generated by the state-averaged complete active space SCF (CASSCF) approach.[46] The MOLPRO program package[47] was employed in these calculations. The averaging was performed for the ground state and the four lowest excited states, taken with equal weights. Two different active spaces, CAS1 and CAS2, were used, comprising 7 and 9 active orbitals, respectively. In the first case, all occupied π-type MOs (two b_1 and one a_2) and four virtual orbitals (one of each a_1, a_2, b_1, and b_2 symmetry type) were included. In the second case additional virtual orbitals of b_1 and a_2 symmetry were included to improve the treatment of states with mixed Rydberg-valence character. All configurations with weights of more than 0.03 in the CASSCF expansion were used as reference in the MRCI calculations. The active orbital space in the MRCI calculations was analogous to the CASSCF space, but included also all occupied MOs. In all calculations the sum of the weights of the reference configurations in the final MRCI expansion was at least 0.9. Corresponding to the two types of active space, CAS1 and CAS2, the two variants of our MRCI/CASSCF calculations are further referred to as MRCI-1 and MRCI-2, respectively.

The aug-cc-pVDZ basis set of Dunning[48,49] augmented by single s- and p-type diffuse functions (C: $\zeta_s=0.01$, ζ_p

TABLE I. Energies (eV) and oscillator strengths of vertical transitions to the low-lying excited singlet states of furan.

Method		Excitation energies					Oscillator strengths		
		$^1A_2$ $(3s)$	$^1B_2$ (V)	$^1B_1$ $(3p)$	$^1A_1$ (V')	$^1A_2$ $(3p)$	$^1B_2$ (V)	$^1B_1$ $(3p)$	$^1A_1$ (V')
EOM-CCSD[a]	Opt.[b]	6.01	6.44	6.53	6.72	6.69	0.166	0.036	<0.001
	Expt.[c]	6.04	6.49	6.56	6.84	6.71	0.167	0.036	<0.001
	$+d$[d]	5.99	6.44	6.52	6.79	6.68	0.167	0.036	<0.001
	$+s,p$[e]	6.03	6.47	6.56	6.83	6.64			
CCSD[f]	ANO	6.04	6.49	6.56	6.86	6.73	0.149	0.041	0.001
	D+7	5.99	6.48	6.51	6.88	6.67	0.144	0.035	<0.001
	T+7	6.11	6.45	6.64	6.82	6.80	0.164	0.035	<0.001
CC3[f]	ANO	5.96	6.35	6.50	6.61	6.65			
CC2[f]	ANO	5.91	6.40	6.42	6.82	6.57	0.149	0.039	0.002
ADC(2)[g]		5.86	6.37	6.35	6.70	6.50	0.148	0.037	0.003
SAC-CI[h]		5.99	6.40	6.45	6.79	6.66	0.185	0.031	<0.001
MRCI-1[a]		5.87	6.59	6.38	6.53				
MRCI-2[a]		5.84	6.44	6.36	6.53				
CASPT2[i]		5.92	6.04	6.46	6.16	6.59	0.154	0.031	0.002
MRCI[j]		5.95	6.76	6.63	6.02	6.41			
DFT[k]		5.97	6.12	6.58	6.76	6.69	0.158	0.036	

[a]This work, see text for details.
[b]CCSD optimized geometry of the ground state.
[c]Experimental ground state geometry (Ref. 50).
[d]Basis set "$+d$," see text for details.
[e]Basis set "$+s,p$," see text for details.
[f]Results and basis set notations from Ref. 22.
[g]Reference 23.
[h]Reference 19.
[i]Reference 25.
[j]Reference 3.
[k]Reference 18.

$=0.02$; O: $\zeta_s=0.02$, $\zeta_p=0.04$) was used for the second row atoms. The hydrogen atoms were described by the standard cc-pVDZ basis set.[48] The five-component representation of the d-functions was adopted in the calculations. The total number of molecular orbitals in the calculations using this basis (further denoted also as cc-pVDZ+) was 155. For purposes of testing we used also the cc-pVDZ+ basis augmented by additional s, p, and d diffuse exponents (C: $\zeta_s=0.006$, $\zeta_p=0.008$, $\zeta_d=0.03$; O: $\zeta_s=0.01$, $\zeta_p=0.02$, $\zeta_d=0.06$).

In the CASSCF MR-CI calculations the C $1s$ and O $1s$ core orbitals were kept frozen, whereas in the EOM-CCSD calculation no orbitals were frozen.

III. RESULTS

The total ground- and excited-states energies obtained in this work for various structures of the furan molecule are summarized in Table XII (Appendix). Here also the available ZPVE corrections are listed. All results to be discussed in the following (excitation energies and various energy differences) can be obtained from the data presented in Table XII. In the following we adopt the nomenclature, in which the adiabatic PES of the singlet states are denoted as S_0, S_1, S_2,.... Here we strictly assume that the S_i surface is formed by the energies obtained as the $(i+1)$th root of the Hamiltonian (irrespective of symmetry) at all nuclear conformations. In the following we will also make use of the spectroscopic terminology, according to which distinct stationary points of a PES (various minima or saddle points) are called "states."

A. Vertical excitations

To make a link to the previous theoretical and experimental work on the electronic excitation in furan and to get a feeling for the accuracy of the present results, we discuss here the vertical transition energies and oscillator strengths in comparison to the earlier data. Only the lowest part of the excitation spectrum is considered.

In Table I we compare our results for the lowest five vertical singlet excitations of furan with the results of CCSD, CC3, and CC2 calculations of Christiansen *et al.*,[21,22] our previous ADC(2) calculations,[23] recent SAC-CI calculations of Wan *et al.*,[19] and DFT calculations of Burcl *et al.*[18] In addition, we include some older CASPT2 results of Serrano-Andrés *et al.*[25] and MRCI results of Palmer *et al.*[3]

Since some of the previous theoretical studies were performed using somewhat different ground-state equilibrium geometries, it seems to be important to clarify first the effect of such differences on the vertical excitation energies and oscillator strengths. To this end, we compare our results for the most commonly used experimental geometry of Mata *et al.*[50] with our results for the optimized geometry, obtained using the CCSD approach (Sec. III B). As can be seen, the results for the two geometries differ only very little for the considered $3s$-, $3p$-Rydberg transitions and the $V(^1B_2)$ valence transition. The energy of the $V'(^1A_1)$ valence transition seems to be more sensitive to a variation of the geometry, showing differences of 0.12 eV for the two sets of parameters.

Another important question is whether our cc-pVDZ+ basis provides for a reliable description of all states under investigation. To check the description of the Rydberg states we preformed two additional calculations. In the first case the cc-pVDZ+ basis was augmented by additional d-type diffuse functions ($+d$ basis), and in the second case by additional s- and p-diffuse functions ($+s,p$ basis). In both cases the changes in the excitation energy of the $^1A_2(3s)$, $^1B_2(V)$, $^1B_1(3p)$, and $^1A_1(V')$ states were negligible, indi-

cating that the diffuse functions in the cc-pVDZ+ basis set yield a good description of these states. Since the present EOM-CCSD approach is equivalent (with respect to the treatment of energies) to the CCSD method used by Christiansen *et al.*,[21,22] we may compare directly our cc-pVDZ+ results to the results of the latter work obtained using ANO, cc-pVDZ, and cc-pVTZ, basis sets augmented by ring-centered diffuse functions (denoted in Ref. 22 as ANO, D+7, and T+7, respectively). The compared results again look very similar, indicating that all these basis sets, including our cc-pVDZ+ basis, are equally adequate for the description of the above four states.

The next issue is the accuracy of the present calculations. As has been established in calibrations with respect to full configuration interaction (FCI) results,[51] the average accuracy of the CCSD approach for the energy of single excitations is about 0.2 eV, the maximum deviation being 0.4 eV. A superior performance was demonstrated for the CC3 model (here the average deviation from FCI is less than 0.1 eV, the maximum deviation is about 0.2 eV). The CC3 results for furan[21,22] should therefore be already quite close to the FCI limit. The present EOM-CCSD results for the above four states differ from the CC3 results on an average by 0.13 eV, the maximum deviation being 0.23 eV for the $^1A_1(V')$ state. A comparable level of accuracy (average deviation from CC3 less than 0.2 eV, maximum deviation less than 0.3 eV) is observed also for the other CC results (CC2 and SAC-CI) listed in Table I. Our earlier ADC(2) calculations[23] reaches the same accuracy mark, yielding results very similar to those of the CC2 scheme. The latter observation is in line with the analysis of the two schemes given in Ref. 52.

The results of the recent DFT calculations of Burcl *et al.*[18] compare to the CC3 data[21,22] equally well, which demonstrates that consistent results can be obtained not only with the theoretically similar (coupled cluster and propagator) approaches. To give further support for this view, we have performed additional MRCI/CASSCF calculations using two different active spaces of improving quality (MRCI-1 and MRCI-2, respectively), as described in Sec. II. The vertical excitation energies obtained in these calculations (Table I) are again in good agreement with the CC3 results.[21,22] As expected, the agreement with CC3 improves from MRCI-1 to MRCI-2 (the average/maximal deviation reduces from 0.13 / 0.24 eV in MRCI-1 to 0.11 / 0.14 eV in MRCI-2), reflecting a convergence of the results with the improvement of the method. By contrast, the CASPT2 results[25] and the older MRCI results[3] show discrepancies of up to 0.5–0.6 eV with respect to the other results in Table I, and thus do not fit so well in the consistent picture drawn above.

The present oscillator strengths for the $V(^1B_2)$ transition, calculated using the EOM-CCSD approach, differ from the LR-CCSD results obtained by Christiansen *et al.*[21,22] This is partly due to the different basis sets used in the present EOM-CCSD calculations. It should, however, be recalled that in contrast to the equivalent treatment of the energies, the two methods differ in the treatment of transition moments (see, for example, discussion in Ref. 53). The oscillator strengths for the $V(^1B_2)$ transition vary between 0.185 and 0.144, depending on the method and the basis set used. The same magnitude of discrepancies is seen for the $3p(^1B_1)$ transition, though the EOM- and LR-CCSD results are in much better mutual agreement here. Finally, all methods compared in Table I predict a negligible oscillator strength for the $V'(^1A_1)$ transition, which may partly be attributable to its considerable doubly-excited character.

Concluding this section we note that an important consensus has been reached in the theoretical description of the lowest $^1A_2(3s)$, $^1B_2(V)$, $^1B_1(3p)$, and $^1A_1(V')$ singlet states of furan. The accuracy of about 0.2 eV of the excitation energies, afforded by several computational methods including the presently used EOM-CCSD method, should establish a reliable basis for investigating the excitation spectrum of furan at a level that accounts for various vibronic and nonadiabatic effects.

B. $\tilde{X}^1A_1$ ground state

The ground-state calculations allow us to estimate the accuracy of our approach by a direct comparison to experiment. Moreover, the ground-state structural and vibrational data are needed for the next stage of our study aiming at the modeling of the vibronic structure of the excitation spectrum.[42]

In Table II we present our CCSD results for the equilibrium ground-state geometry of furan in comparison with the experimental data of Nygaard *et al.*[54] and results of some earlier theoretical studies. The latter comprise our previous second-order Møller–Plesset perturbation theory (MP2) calculations using the cc-pVDZ basis set,[34] the MP2 calculations of Mellouki *et al.*[55] using the cc-pVTZ basis, and the augmented ''triple zeta'' (TZ2P+) basis set DFT calculations of Burcl *et al.*[18] All theoretical results agree fairly well with the experimental data. The best agreement with experiment is seen for the MP2/cc-pVTZ (Ref. 55) and DFT/TZ2P+ (Ref. 18) results.

To study the basis set effects in the CCSD geometry optimization, we have performed additional calculations using the standard cc-pVDZ and the cc-pVTZ basis sets. As seen from the calculated values of the geometrical parameters, all three basis sets provide a roughly comparable accuracy, though it may be noted that the bond lengths appear to be slightly overestimated at the ''double zeta'' and slightly underestimated at the ''triple zeta'' level.

The calculated ground-state harmonic vibrational frequencies are given in Table III together with the recent experimental and theoretical (MP2/cc-pVTZ) results of Mellouki *et al.*[55] The table includes also our previous MP2/cc-pVDZ results[34] and the older experimental data of Rico *et al.*[56] In the present work we adopt the revised nomenclature of furan vibrational modes of Mellouki *et al.*[55] instead of the obsolete and less transparent nomenclature of Lord and Miller,[57] which was used in our previous work.[23,34] All theoretical results are seen to be in very good agreement with each other, and there is also a good overall agreement with experiment. An exception are the high-frequency hydrogenic modes, for which the calculations systematically overestimate the frequencies. As for the geometries, neither a pro-

TABLE II. Calculated and experimental ground-state ($\tilde{X}\,^1A_1$) equilibrium geometry of furan (bond lengths in Å and angles in deg, Fig. 1).

	CCSD cc-pVDZ+	CCSD cc-pVDZ[a]	CCSD cc-pVTZ[b]	MP2 cc-pVDZ[c]	MP2 cc-pVTZ[d]	DFT TZ2P+[e]	Expt.[f]
Bond lengths							
$O-C_2$	1.371	1.365	1.354	1.364	1.359	1.361	1.362
C_2-C_3	1.369	1.368	1.349	1.378	1.364	1.358	1.361
$C_3-C_{3'}$	1.451	1.448	1.433	1.436	1.426	1.435	1.431
C_2H_2	1.087	1.088	1.069	1.088	1.074	1.077	1.075
C_3-H_3	1.089	1.089	1.070	1.089	1.075	1.078	1.077
Angles							
$C_{2'}-O-C_2$	106.6	106.5	106.5	106.7	106.7	106.8	106.7
$O-C_2-C_3$	110.8	111.1	110.9	110.8	110.6	110.6	110.7
$C_2-C_3-C_{3'}$	105.9	105.7	105.9	105.9	106.1	106.0	106.0
$O-C_2-H_2$	115.8	115.8	116.1	115.8	115.9	116.0	115.9
$C_2-C_3-H_3$	126.3	126.3	126.5	126.3	126.1	126.4	126.1

[a]E_0 (CCSD) = −229.390 777 Hartree.
[b]E_0 (CCSD) = −229.667 486 Hartree.
[c]Reference 34.
[d]Reference 55.
[e]Reference 18.
[f]Reference 54.

nounced basis set effect nor a major dependence on the method used is seen in the calculated frequencies. One may note a slight improvement of the results for the modes ν_6 and ν_{11} obtained using the CCSD method with respect to the MP2 level.

C. $^1A_2(3s)$ state

The present CCSD geometry optimization predicts for the $^1A_2(3s)$ state of furan only one stationary point in the vicinity of the ground-state equilibrium geometry. At this point the molecule has a symmetric C_{2v} structure like in the ground state. The electronic configuration corresponds to a single electron excitation out of the highest occupied molecular orbital, π_3 (a_2), into an orbital of a_1 symmetry. The large values of the second moments of the electronic charge (Table IV) support the $3s$ Rydberg assignment.

The optimized geometrical parameters of the $^1A_2(3s)$ state are given in Table V together with the previous DFT

TABLE III. Calculated and experimental frequencies (cm^{-1}) for the $\tilde{X}\,^1A_1$ ground state of furan.

Mode[a]	CCSD cc-pVDZ+	MP2 cc-pVDZ[b]	MP2 cc-pVTZ[c]	Expt.[d]	Expt.[c]
a_1 modes					
ν_1	3312	3332	3326	3167	3169
ν_2	3283	3306	3300	3140	3140
ν_3	1546	1520	1510	1491	1491
ν_4	1427	1430	1421	1384	1385
ν_5	1165	1164	1166	1140	1140
ν_6	1082	1116	1114	1066	1067
ν_7	1011	1021	1026	995	995
ν_8	878	875	879	871	870
a_2 modes					
ν_9	874	843	868	863	864
ν_{10}	739	720	726	728	722
ν_{11}	599	599	613	613	600
b_1 modes					
ν_{12}	855	824	839	838	838
ν_{13}	761	756	761	745	745
ν_{14}	606	628	632	603	603
b_2 modes					
ν_{15}	3304	3326	3318	3161	3161
ν_{16}	3271	3295	3290	3129	3130
ν_{17}	1617	1585	1578	1556	1558
ν_{18}	1289	1282	1292	1267	1267
ν_{19}	1216	1249	1248	1180	1181
ν_{20}	1062	1059	1066	1040	1043
ν_{21}	884	878	884	873	873

[a]Nomenclature of Mellouki *et al.* (Ref. 55).
[b]Reference 34.
[c]Reference 55.
[d]Reference 56.

TABLE IV. One-electron properties (a.u.) for the low-lying excited singlet states of furan at their equilibrium geometries.[a]

State	Configuration	$\langle z \rangle$	$\langle x \rangle$	$\langle y \rangle$	$\langle x^2 \rangle$	$\langle y^2 \rangle$	$\langle z^2 \rangle$
$\tilde{X}\ ^1A_1$	Ground state	0.261			24.4	137.1	135.0
$^1A_2\ (3s)$	$\pi_3 \rightarrow 3s$	−0.098			40.9	148.6	154.7
$^1B_2\ (V)$	$\pi_3 \rightarrow \pi_4^*$	0.747			31.3	137.2	145.0
$^1A'\ (V)$	$\pi_3 \rightarrow \pi_4^*$	0.825	0.0	−0.343	28.7	137.7	147.1
$^1B_1\ (3p)$	$\pi_3 \rightarrow 3p$	−0.075			35.9	180.0	149.9
$^1A_1\ (V')$	$\pi_3 \rightarrow \pi_5^*$, $\pi_2 \rightarrow \pi_4^*$ π_2, $\pi_3 \rightarrow \pi_4^*$, π_5^*	0.342			25.6	141.6	144.1
$^1A'\ (V')$	$\pi_3 \rightarrow \pi_5^*$, $\pi_2 \rightarrow \pi_4^*$ π_2, $\pi_3 \rightarrow \pi_4^*$, π_5^*	0.335	−0.519	0.0	26.3	141.6	142.4
$^1A\ (V')$	$\pi_3 \rightarrow \pi_5^*$, $\pi_2 \rightarrow \pi_4^*$ π_2, $\pi_3 \rightarrow \pi_4^*$, π_5^*	0.209			26.1	140.4	143.9

[a]See text for further details on the notation of the states.

results of Burcl *et al.*[18] The two sets of results are seen to be in good agreement. The $^1A_2(3s)$ excited-state geometry differs from that in the ground state mainly in some elongation of the C_2-C_3 ($C_{2'}-C_{3'}$) bond and a contraction of the $C_3-C_{3'}$ bond. This is consistent with the picture of an electron excitation out of the π-type MO associated with the C_2-C_3 ($C_{2'}-C_{3'}$) double bond into a nonbonding $3s$ Rydberg orbital.

The corresponding vibrational frequencies are given in Table VI. The absence of any imaginary frequencies confirms that the located stationary point [$^1A_2(3s)$ state] is indeed a true minimum of the S_1 adiabatic PES. Many vibrational frequencies do not differ very much from those in the ground state, indicating a similarity of the local topological properties of the S_0 and S_1 PES. The largest reduction of the vibrational frequency is found for the b_1 mode ν_{14}, the three b_2 modes ν_{17}, ν_{19}, and ν_{21} and the a_2 mode ν_{11}.[58] Unfortunately, no comparison can be made to the results of Burcl *et al.*,[18] since in that work no assignment of the vibrations has been given.

The present adiabatic (0–0) energy of the $3s(^1A_2)$ transition is 5.84 eV (Table VII). The corresponding value including ZPVE corrections for the ground and the excited states is 5.79 eV. This value, differing somewhat from our previous estimate of the 0–0 transition energy of 5.53 eV,[23] is in good agreement with the results of Christiansen and Jørgensen[21] (5.89 eV), and in even better agreement with the results of Burcl *et al.*[18] (5.83 and 5.80 eV, respectively).

D. $^1B_2(V)$ state

The stationary point of the S_2 PES associated with a symmetric C_{2v} structure [$^1B_2(V)$ state], appears to be a saddle point rather than a true minimum (Table V). This follows from the fact that there is one imaginary frequency for the ν_{21} (b_2) mode, describing an in-plane distortion of the molecule (Table VI). This surprising finding is at variance with previous theoretical results. The DFT calculations of Burcl *et al.*[18] here predict an out-of-plane distortion of the molecule, whereas on the basis of their CC calculations Christiansen and Jørgensen[21] do not detect any structural instability at all in the $^1B_2(V)$ state.[59] These differences of the theoretical predictions for the $^1B_2(V)$ state are analyzed in more detail in Sec. IV A.

TABLE V. Calculated equilibrium geometry of furan (bond lengths in Å and angles in deg) in the ground and low-lying excited singlet states associated with a C_{2v} type of molecular structure (Fig. 1).

	$\tilde{X}\ ^1A_1$	$^1A_2\ (3s)$		$^1B_2\ (V)$		$^1B_1\ (3p)$		$^1A_1(V')$
	CCSD[a]	CCSD[b]	DFT[c]	CCSD[b]	DFT[c]	CCSD[b]	DFT[c]	CCSD[b]
Bond lengths								
O–C2	1.371	1.352	1.346	1.387	1.396	1.354	1.347	1.378
C2–C3	1.369	1.417	1.405	1.443	1.439	1.419	1.407	1.460
C3–C3′	1.451	1.393	1.380	1.383	1.370	1.398	1.384	1.464
C2–H2	1.087	1.091	1.080	1.089	1.078	1.091	1.079	1.085
C3–H3	1.089	1.092	1.081	1.088	1.077	1.090	1.070	1.088
Angles								
C2′–O–C2	106.6	106.2	106.0	104.7	103.5	106.7	106.5	109.6
O–C2–C3	110.8	111.2	111.0	111.3	111.6	110.8	110.8	109.6
*C*2–C3–C3′	105.9	105.7	106.0	106.4	106.7	105.8	106.0	105.6
O–C2–H2	115.8	116.4	116.6	116.0	116.0	117.1	117.1	116.6
C2C3–H3	126.3	125.4	125.3	124.8	124.6	124.6	124.8	126.5

[a]CCSD, this work.
[b]EOM-CCSD, this work.
[c]Reference 18.

TABLE VI. Calculated vibrational frequencies (cm^{-1}) for the ground and low-lying excited singlet states of furan.

Mode	ν	$\tilde{X}\,^1A_1$	$^1A_2\,(3s)$	$^1B_2\,(V)$	$^1B_1\,(3p)$	$^1A_1\,(V')$	$^1A'\,(V)$
$a_1\,(a')$[a]	1	3312	3260	3310	3284	3332	3336
	2	3283	3228	3295	3256	3303	3301
	3	1546	1532	1544	1518	1446	3279
	4	1427	1486	1441	1474	1407	3265
	5	1165	1177	1118	1166	1079	1458
	6	1082	1117	1089	1114	1066	1432
	7	1011	1048	972	1051	974	1360
	8	878	873	767	876	769	1256
$b_2\,(a')$[a]	15	3304	3266	3297	3254	3451	1209
	16	3271	3234	3277	3227	3305	1085
	17	1617	1422	1352	1402	2914	1037
	18	1289	1301	1274	1296	1404	962
	19	1216	1050	956	1047	1261	822
	20	1062	990	858	990	1053	730
	21	884	757	629 *i*	777	863	516
$a_2\,(a'')$[a]	9	874	962	841	986		774
	10	739	854	635	868		629
	11	599	429	320	519		466
$b_1\,(a'')$[a]	12	855	888	684	922		313
	13	761	733	500	775		400 *i*
	14	606	377	72	476		2174 *i*

[a]For the $^1A'\,(V)$ state.

In spite of the disagreement of our results and those of Burcl *et al.*[18] in regard to the symmetry breaking in the $^1B_2(V)$ state, there is a rather good agreement for the geometrical parameters for the C_{2v} structure (Table V). The most notable difference here is the value of the $C_2{-}O{-}C_{2'}$ angle, where our result is 1.2° larger that of Burcl *et al.*[18] As could be expected in view of the valence character of the $^1B_2(V)$ state, the geometry relaxation pattern here is somewhat different from the case of the Rydberg $^1A_2(3s)$ state. The most characteristic geometrical modifications are an elongation of the $O{-}C_2$ ($O{-}C_{2'}$) and $C_2{-}C_3$ ($C_{2'}{-}C_{3'}$) bonds, a strong contraction of the $C_3{-}C_{3'}$ bond and a reduction of the $C_2{-}O{-}C_{2'}$ angle.

Another interesting observation concerning the vibrational analysis of the $^1B_2(V)$ state (Table VI) is the marked frequency reduction of many b_1, b_2, and a_2 modes as compared to the ground state frequencies. This is particularly striking in the case of the $\nu_{14}\,(b_1)$ and $\nu_{11}\,(a_2)$ modes, for which the frequencies are reduced roughly by a factor of 8 and 2, respectively.

The electronic configuration of the $^1B_2(V)$ state is characterized by the excitation of an electron from the highest occupied $\pi_3\,(a_2)$ MO into a virtual orbital of b_1 symmetry. The latter can be of π^*-valence or of p-Rydberg type, and consequently there is the possibility of mixing of valence and Rydberg character in the $^1B_2(V)$ state—an issue, that has

TABLE VII. Adiabatic excitation energies E_{0-0} (eV) of the low-lying singlet transitions of furan.

Transition	EOM-CCSD (this work)			ADC(2)[a]	CCSD[b]	DFT[c]		Expt.
$\tilde{X}\,^1A_1\rightarrow$	Δ_E[d]	Δ_E (ZPVE)[e]	Model[f]	Model[f]	Δ_E[d]	Δ_E[d]	Δ_E (ZPVE)[e]	
$^1A_2\,(3s)$	5.84	5.79	5.84	5.53	5.89	5.83	5.80	5.91[g]
$^1B_2\,(V)$	6.11	5.91	6.12	6.12	6.05[h]	5.79		6.04[i]
$^1A'\,(V)$	6.07	5.85	6.08					
$^1B_1\,(3p)$	6.37	6.34	6.37	6.22	6.44	6.43	6.42	6.47[j]
$^1A_1\,(V')$	6.36		6.38	6.37	6.13[h]			
$^1A'\,(V')$	6.34							
$^1A\,(V')$[k]	6.34							

[a]Reference 23.
[b]Reference 21.
[c]Reference 18.
[d]Difference of the total energies for the equilibrium configurations of the initial and final states.
[e]Same as in footnote d, but with zero-point vibration energies (ZPVE) corrections for both states.
[f]Predictions of the linear vibronic coupling model, see text for details.
[g]Reference 7.
[h]Obtained from the data of Ref. 21 as a sum of the best estimated vertical excitation energy and the relaxation energy correction ($V{-}A$).
[i]Band maximum, Ref. 3.
[j]References 3 and 17.
[k]The geometry optimization is not fully converged.

often been discussed in the previous theoretical work.[23–25,60] As can be seen from the second moments of the charge distribution (Table IV), the $^1B_2(V)$ state is clearly quite different from the typical $^1A_2(3s)$ and $^1B_1(3p)$ Rydberg states.

The present energy of the $V(^1B_2)$ adiabatic transition is 6.11 eV (or 5.91 eV upon ZPVE corrections). This is in excellent agreement with our previous estimate of 6.12 eV (Ref. 23) and the result of Christiansen and Jørgensen[21] (6.05 eV), whereas the value of 5.79 eV obtained by Burcl *et al.*[18] seems to be too small. With respect to the adiabatic correction the present (0.33 eV) and the two previous results (0.27 eV and 0.33 eV, respectively) agree very well. Finally, we have to recall, that since the $^1B_2(V)$ state is a saddle point on the S_2 adiabatic PES, the 0–0 transition energies given above can be viewed only as some upper limit estimates.

E. $^1A'(V)$ state

Using the coordinates defined at the C_{2v} structure of the $^1B_2(V)$ state and proceeding along the ν_{21} (b_2) imaginary frequency mode, we located another stationary point corresponding to a planar C_s structure with nonequivalent bonds and angles [Fig. 2(A), Table VIII]. This structure is energetically only slightly below the C_{2v} saddle point (Table VII), and is characterized by a stabilization energy of 0.04 eV (or 0.06 eV upon ZPVE corrections). The electronic configuration and the one-electron properties given in Table IV indicate that this state is of the same type as the $^1B_2(V)$ saddle point of S_2. We will designate the new C_s structure as $^1A'(V)$.

Further analysis of the results reveals a surprising fact, namely, that the $^1A'(V)$ state is the lowest excited singlet state of furan at that C_s stationary point (Table XII). This means that the $^1A'(V)$ state belongs to the S_1 adiabatic PES, and consequently an intersection of the S_2 and S_1 PES must occur on the path from the C_{2v} to the C_s structure. Indeed, here the second state is $^1A''(3s)$, which correlates with the $^1A_2(3s)$ Rydberg state at the C_{2v} configuration of the molecule. Since the $^1A''(3s)$ state lies only 0.02 eV above the $^1A'(V)$ state, one can deduce the close proximity of the C_s structure to the structure of the molecule at the intersection point. The intersection energy should be between 6.07 and 6.09 eV with respect to the ground-state minimum.

The strikingly different character of the obtained C_s molecular structure in comparison to the ground-state equilibrium configuration is reflected by the strongly different $O–C_2$ and $O–C_{2'}$ bond lengths. Whereas one of the bonds elongates to 1.50 Å, the other one contracts to 1.32 Å, thereby approaching the typical lengths of a single and a double chemical bond, respectively. Another modification is the lengthening of the C–C bond adjacent to the shorter O–C bond to a value of 1.46 Å. The other two C–C bonds experience only minor elongations. It should be noted that there are, of course, two equivalent C_s structures, lying on either side of the C_{2v} saddle point, symmetric with respect to the inversion of the b_2 relaxation coordinate.

An inspection of the vibrational frequencies calculated for the $^1A'(V)$ state (Table VI) reveals that also the C_s structure is not a minimum but rather a saddle point of the S_1 PES. Two of the a'' vibrational modes, corresponding to out-of-plane distortions of the molecule, are characterized by imaginary frequencies. The value $2174i$ cm^{-1} of one of these frequencies seems to be unphysically large. Lacking another reasonable explanation, we have to assume that this result is a computational ''artifact,'' probably due to some numerical instability.

TABLE VIII. Calculated equilibrium geometries of furan (bond lengths in Å and angles in deg) in the low-lying excited singlet states associated with C_s and C_2 types of molecular structures (Fig. 2).

	$^1A'(V)$	$^1A'(V')$	$^1A(V')$[a]
Bond lengths			
$O–C_2$	1.320	1.388	1.376
$C_2–C_3$	1.455	1.455	1.462
$C_3–C_{3'}$	1.404	1.467	1.458
$C_2–H_2$	1.091	1.090	1.089
$C_3–H_3$	1.089	1.088	1.090
$O–C_{2'}$	1.500		
$C_{2'}–C_{3'}$	1.427		
$C_{2'}–H_{2'}$	1.086		
$C_{3'}–H_{3'}$	1.087		
Valence angles			
$C_{2'}–O–C_2$	104.8	109.9	109.9
$O–C_2–C_3$	112.8	108.1	109.6
$C_2–C_3–C_{3'}$	107.1	106.1	105.6
$O–C_2–H_2$	117.3	114.9	115.5
$C_2–C_3–H_3$	124.1	126.4	125.3
$O–C_{2'}–C_{3'}$	108.8		
$C_{2'}–C_{3'}–C_3$	106.5		
$O–C_{2'}–H_{2'}$	113.9		
$C_{2'}–C_{3'}–H_{3'}$	125.8		
Dihedral angles			
$C_3–C_2–O–C_{2'}$		13.7	−0.2
$C_{3'}–C_{2'}–O–C_2$		−13.7	−0.2
$H_2–C_2–O–C_{2'}$		167.5	−164.2
$H_{2'}–C_{2'}–O–C_2$		−167.5	−164.2
$H_3–C_3–C_2–O$		172.1	167.1
$H_{3'}–C_{3'}–C_{2'}–O$		−172.1	167.1

[a]The geometry optimization is not fully converged.

Further attempts to search for stationary points below the $^1A'(V)$ saddle point led only to the C_{2v} minimum of the S_1 PES [$^1A_2(3s)$ state]. No other stationary point could be found by an out-of-plane distortion of the C_s structure, as is suggested by the a'' imaginary modes at the $^1A'(V)$ saddle point. Of course, this does not exclude the existence of a shallow local minimum that we failed to locate. The search for minima here is difficult because of the extreme flatness of the S_1 PES in the considered region. Another problem is the tremendous increase of the computational effort due to the low (C_1) symmetry of the system.

F. $^1B_1(3p)$ state

According to the present results the $^1B_1(3p)$ state is, both vertically and at its own equilibrium geometry, the third lowest singlet state of furan. It is a typical Rydberg state, characterized by relatively large second moments (Table IV) and small relaxation changes in the geometrical parameters.

According to the present results, the optimized molecular structure has C_{2v} symmetry and is nearly identical to the structure of the $^1A_2(3s)$ Rydberg state (Table V). Our geometrical parameters for the $^1B_1(3p)$ state are seen to be in good agreement with those of Burcl *et al.*[18] There is a high degree of similarity between the vibrational frequencies of the $^1B_1(3p)$ and $^1A_2(3s)$ states (Table VI). The agreement is especially good for the a_1 and b_2 modes. The frequencies of some b_1 and a_2 modes, on the other hand, are seen to be closer to the ground-state values.

As seen from Table VII, the present energy of the $3p(^1B_1)$ adiabatic transition is 6.37 eV (or 6.34 eV upon ZPVE correction). This is somewhat less than predicted by the DFT calculations of Burcl *et al.*[18] (6.43 and 6.42 eV, respectively) and the value estimated by Christiansen and Jørgensen[21] (6.44 eV).

G. $^1A_1(V')$ state

The $^1A_1(V')$ valence state is one of the most complex states in the spectrum of furan. It has a strongly mixed character, including $\pi-\pi^*$ configurations of two types (Fig. 1), and, moreover, considerable contributions of various doubly-excited configurations. Understandably, this state has been a particular challenge to the theoretical methods (see, e.g., discussion in Refs. 22 and 23). Here the shortcomings of theoretical schemes that disregard the doubly-excited configurations (e.g., CIS and time-dependent DFT) or treat them only through low-order of perturbation theory [e.g., ADC(2) and CC2] are obvious. In the EOM-CCSD approach, the double excitations are treated consistently through first-order of perturbation theory (PT), that is, at a lower level of theory than the single excitations. In view of the mixing of the two configuration types in the $^1A_1(V')$ state a somewhat reduced accuracy has to be expected here. Another complication is due to the strong dependence of the $^1A_1(V')$ state on the molecular geometry: at the ground-state equilibrium geometry the present calculations place the $^1A_1(V')$ state energetically at the fifth position, whereas it is the third state at its own equilibrium conformation.

According to the present results, the $^1A_1(V')$ PES has a stationary point corresponding to a C_{2v} structure (Table V). The geometrical parameters at this point differ markedly from those of the other excited states. As compared to the ground-state equilibrium geometry, the main structural effects here are the elongation of the C_2-C_3 ($C_{2'}-C_{3'}$) and $C_3-C_{3'}$ bonds, as well as a 3° increase of the $C_2-O-C_{2'}$ angle.

The present energy of the adiabatic $V'(^1A_1)$ excitation is 6.36 eV (Table VII). This implies a geometry relaxation correction of 0.36 eV, which is in fair agreement with the result of Christiansen and Jørgensen[21] (0.44 eV). However, their best estimate for the 0–0 transition (6.13 eV) is by 0.2 eV lower than our result. The previous ADC(2) results for the 0–0 transition energy and the relaxation correction (6.37 and 0.33 eV, respectively) agree remarkably well with the present EOM-CCSD values. No structural study for the $^1A_1(V')$ state has been reported in the work of Burcl *et al.*[18]

Unfortunately, we did not succeed in computing other frequencies than those of the a_1 and b_2 modes for the $^1A_1(V')$ state. For the modes of b_1 and a_2 symmetry our calculations failed for some technical reasons related to the ACES II program.[61] While the frequencies for the a_1 modes are quite similar to the ground-state values, one can see a strong frequency increase for the b_2 modes ν_{17} and ν_{18}. Our results show no imaginary frequencies for the a_1 and b_2 modes, so that we can safely exclude the possibility of an in-plane instability of the $^1A_1(V')$ state. However, our vibrational analysis is not complete, and one should check for the possibility of out-of-plane distortions before drawing conclusions about the type of that stationary point. It should be noted that some (unspecified) symmetry breaking of the $^1A_1(V')$ state has been reported by Christiansen and Jørgensen.[21]

To check for possible distortions along the b_1 and a_2 out-of-plane coordinates, we carried out additional geometry optimizations without the C_{2v} symmetry constraint. In the former case, the C_{2v} structure of the $^1A_1(V')$ state was distorted to a C_s structure by incrementing the b_1 coordinate. In the latter case, some steps were taken along the a_2 coordinate, resulting in a C_2 structure. For both the C_s and C_2 trial structures a full geometry optimization was performed within the respective point group symmetries. As a result, two new stationary points have been located with energies slightly lower than that of the initial C_{2v} structure, indicating that C_{2v} structure of the $^1A_1(V')$ state is, in fact, a saddle point of order two.

H. $^1A'(V')$ state

The optimized geometrical parameters for the C_s structure [$^1A'(V')$ state] are given in Table VIII and visualized in Fig. 2(B). Most of these geometrical parameters do not differ from those of the $^1A_1(V')$ state. The principal new aspect here is, of course, that the molecule becomes nonplanar. However, as seen from the dihedral angles, the extent of the out-of-plane distortion is rather modest. The small geometry changes are consistent with a small value of the stabilization energy, being 0.02 eV. Interestingly, in contrast to the parent $^1A_1(V')$ state on the S_3 PES, the $^1A'(V')$ state belongs to the S_2 PES, which indicates that a crossing of the S_3 and S_2 PES takes place along the path of geometry relaxation. The electronic configuration of the $^1A'(V')$ state and other characteristics of its electronic structure (Table IV) are quite similar to those seen for the $^1A_1(V')$ state.

It should be noted that a C_s structure resulting from a symmetry breaking of the $^1A_1(V')$ state has been reported by Christiansen and Jørgensen,[21] predicting, however, a much larger stabilization energy (0.13 eV). Unfortunately, no structural data have been given in the latter work, so that no comparison or comments can be made at the present stage.

I. $^1A(V')$ state

The C_2 stationary point is obtained by geometry relaxation along an a_2 coordinate beginning at the $^1A_1(V')$ saddle point. The structural parameters of the furan molecule at the C_2 point [$^1A(V')$ state] are shown in Fig. 2(C) and in Table VIII. It has to be noted that our optimization procedure did

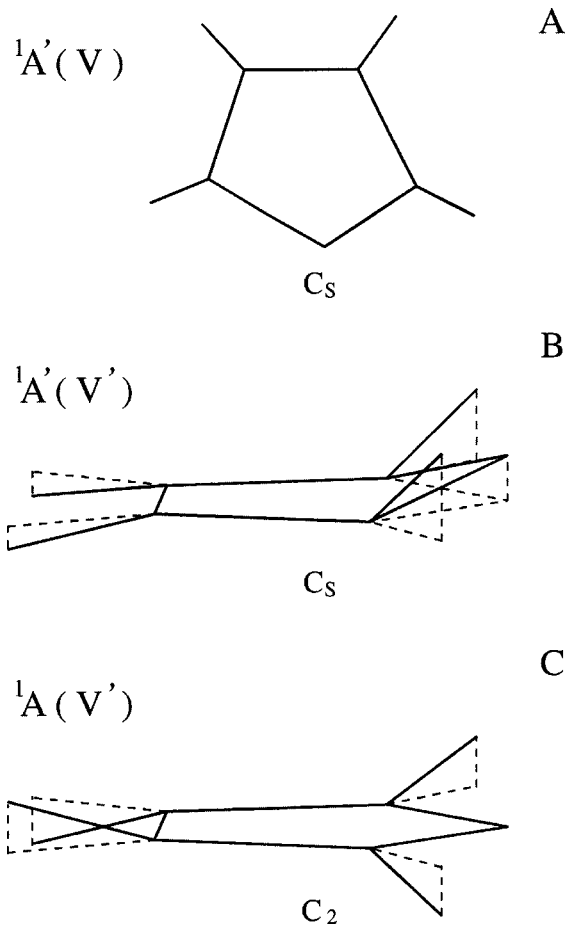

FIG. 2. Molecular structure of furan in the $^1A'(V)$, $^1A'(V')$, and $^1A(V')$ states.

not fully converge here and the results in Table VIII correspond, in fact, to the last point that we managed to obtain. The root mean square (RMS) gradient at this point is 2×10^{-3} Hartree/Bohr, which is still above the otherwise required RMS threshold value of 1×10^{-4} Hartree/Bohr. The optimization failure is probably due to specific shortcomings of the computer code.[61]

Again, the geometric parameters in the $^1A(V')$ state are quite similar to those in the $^1A_1(V')$ state, except for the out-of-plane deformation. Also, the electronic structures of the two states are rather similar to each other (Table IV). A value of 0.02 eV was obtained for the stabilization energy of the $^1A(V')$ state. Like the $^1A'(V')$ state, the $^1A(V')$ state belongs to the S_2 PES.

Since no vibrational analysis could be performed for the C_s and C_2 stationary points [$^1A'(V')$ and $^1A(V')$ states, respectively], it still remains unclear, whether these stationary points are true minima.

IV. DISCUSSION

The major findings of this work deserve a more detailed analysis in the view of their spectroscopic importance. First of all, this concerns the in-plane instability of the $^1B_2(V)$ valence state, the low-lying conical intersection of the S_1 and S_2 potential energy surfaces and the out-of-plane instability of the $^1A_1(V')$ state. A clarification of the various vibronic coupling mechanisms underlying these effects is the key to the understanding of the excitation spectrum of furan and related heteroaromatic molecules.

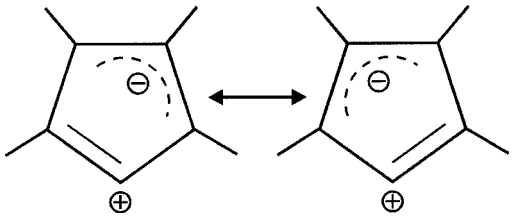

FIG. 3. The valence-bond schemes contributing to the $^1A_1(V')$ and $^1B_2(V)$ valence states (plus and minus linear combinations, respectively).

A. Symmetry breaking in the $^1B_2(V)$ state

Our calculations for the $^1B_2(V)$ state predict a new type of symmetry breaking in furan, namely, an in-plane deformation of its C_{2v} structure. Interestingly, this type of instability has never been mentioned in previous studies of five-membered (hetero)cyclic compounds. To the best of our knowledge, the only type of symmetry breaking predicted for these molecules is an out-of-plane distortion. For example, such nonplanar symmetry breaking of the $^1B_2(V)$ state was suggested for furan,[18] thiophene,[62] and cyclopentadiene.[63]

The driving force for this so-called $B_2\times b_2$ instability is obviously a vibronic interaction with a higher lying A_1 state which in the present case is the $^1A_1(V')$ valence state. It should be admitted that the idea of vibronic coupling between the $^1B_2(V)$ and the $^1A_1(V')$ valence states in five-membered ring molecules is not new. For example, Negri and Zgierski[62] obtained theoretical evidence for such a coupling in thiophene. However, in the latter case the effect was apparently not strong enough to cause a symmetry breaking.

Though at the first glance the in-plane distortion of the molecule looks quite unusual, it can be rationalized already by rather elementary considerations. As seen from the optimized geometries and the atomic charges, the resulting C_s structures resemble very much two of the valence-bond schemes arising in the context of chemical resonance theory (Fig. 3). It can be shown using a transformation to an atomic orbital basis within the Hückel approximation that the two valence schemes in Fig. 3 contribute to the wave functions of $^1A_1(V')$ and $^1B_2(V)$ states as symmetric and antisymmetric linear combinations, respectively. The $^1B_2(V)$ and $^1A_1(V')$ states can therefore be considered as ''resonance hybrids'' formed by these two and possibly further schemes. A displacement from the C_{2v} structure along the b_2 coordinate allows the states to mix, whereupon the energy levels split further apart. Obviously the distortion adjusts the molecular structure to the electronic configuration associated with one of the resonance scheme, making that structure energetically more favorable than the other.

Our results are at variance with those of Burcl *et al.*[18] predicting a nonplanar structure for the $^1B_2(V)$ state on the basis of DFT/TZ2P+ calculations. The absence of an out-of-plane instability is also supported by the recent CC calculations of Christiansen and Jørgensen.[21,59] What could be the reason for the differing results of the DFT calculation? Ac-

TABLE IX. Calculated frequencies (cm^{-1}) of the nontotally symmetric vibrational modes in the $^1B_2$ (V) state of furan: test of different basis sets and theoretical methods.

	CIS			EOM-CCSD	
	STO-3G	6-31+G*	cc-pVDZ+	6-31+G*	cc-pVDZ+
a_2 modes	990	960	961	765	841
	652	714	731	525	635
	443	389	403	227	320
b_1 modes	789	727	853	577	684
	198	350	633	242*i*	500
	449*i*	691*i*	347	2835*i*	73
b_2 modes	3744	3492	3454	3309	3297
	3706	3452	3425	3280	3277
	1485	1448	1435	1375	1352
	1378	1392	1376	1294	1274
	1003	1088	1083	980	956
	947	979	980	866	858
	306	803	806	756*i*	629*i*

cording to computational tests we suggest that the finding of an out-of-plane instability in the $^1B_2(V)$ state must be seen as a theoretical artifact caused by a lack of diffuse basis functions. In Table IX we present results of calculations illustrating that conclusion. We here compare the frequencies of the nontotally symmetric vibrations at the optimal structure of the $^1B_2(V)$ state, computed at the CIS and EOM-CCSD level using the STO-3G, 6-31+G*, and the present cc-pVDZ+ basis sets. As can be seen, the imaginary frequencies of the b_1 out-of-plane modes found with the STO-3G and 6-31+G* basis sets disappear, if the larger cc-pVDZ+ basis is employed. That observation holds for both the CIS and EOM-CCSD calculations. In comparison to the 6-31+G* basis set, the cc-pVDZ+ basis includes one more set of diffuse functions on the second-row atoms, which is crucial for the correct description of the mixed valence-Rydberg character of the $^1B_2(V)$ state. Apparently, the cc-pVDZ+ basis set represents something like a minimal standard for the treatment of the $^1B_2(V)$ state. The basis sets used in the work of Christiansen and Jørgensen[21] are of comparable or even better quality, and consequently the $^1B_2(V)$ state is also planar in their case. On the other hand, smaller (less diffuse) basis sets like the TZ2P+ set of Burcl *et al.*[18] seem to overestimate the valence character of the $^1B_2(V)$ state and fail to describe neighboring Rydberg states properly, which, introducing unphysical couplings, may be the reason for the appearance of an out-of-plane instability.

Another interesting observation to be seen in the data in Table IX is that the in-plane $B_2 \times b_2$ instability (imaginary frequencies of the b_2 modes) arises only at the EOM-CCSD level, but is absent in the CIS results. This strongly supports our view that the in-plane instability reflects a coupling between the $^1B_2(V)$ and $^1A_1(V')$ states. The $^1A_1(V')$ state, having significant double-excitation character, cannot adequately be described at the CIS level, so that, in particular, the above coupling mechanism is not accounted for. The EOM-CCSD method, on the other hand, treats double excitations consistently through first order of perturbation theory,

TABLE X. Vibronic coupling constants for the totally symmetric modes (κ) and for the nontotally symmetric modes (λ) in the low-lying excited singlet states of furan.

	$^1A_2$ (3s)		$^1B_2$ (V)		$^1A_1$ (V')	$^1B_1$ (3p)	$^1A_2$ (3p)
	κ	$\lambda(^1A_2-^1B_2)$	κ	$\lambda(^1B_2-^1A_1)$	κ	κ	κ
a_1 modes							
ν_3	−0.155		−0.192		−0.252	−0.169	−0.166
ν_4	0.130		0.213		0.107	0.129	0.129
ν_5	−0.002		−0.063		−0.199	−0.006	−0.026
ν_6	0.107		0.067		−0.017	0.075	0.122
ν_7	0.044		0.105		0.032	0.027	0.050
ν_8	−0.056		−0.071		0.016	−0.048	−0.039
b_1 modes							
ν_{13}		0.045					
ν_{14}		0.099					
b_2 modes							
ν_{17}				0.106			
ν_{18}				0.064			
ν_{19}				0.200			
ν_{20}				0.079			
ν_{21}				0.071			

and hence, yields a qualitatively correct description of the $^1A_1(V')$ state and its interactions with the other states. However, here the question remains, why that in-plane instability of the $^1B_2(V)$ state was not detected in the CC study of Christiansen and Jørgensen.[21] It is conceivable that these authors have simply overlooked this type of distortion, since no vibrational analysis was carried out. Another explanation is the use of the CC2 model in the geometry optimization. The CC2 method treats the doubly-excited configurations through zeroth order only and one may thus encounter similar problems as in the CIS treatment in the description of the $^1A_1(V')$ state.

$$\mathbf{H}=H_o\mathbf{1}+\begin{pmatrix} E(A_2)+\sum_{s\in a_1}\kappa_s^1 Q_s & \sum_{s\in b_1}\lambda_s^{12}Q_s & 0 \\ \sum_{s\in b_1}\lambda_s^{12}Q_s & E(B_2)+\sum_{s\in a_1}\kappa_s^2 Q_s & \sum_{s\in b_2}\lambda_s^{23}Q_s \\ 0 & \sum_{s\in b_2}\lambda_s^{23}Q_s & E(A_1)+\sum_{s\in a_1}\kappa_s^3 Q_s \end{pmatrix}. \tag{1}$$

In this expression **1** is a (3×3) unit matrix, $E(A_2)$, $E(B_2)$, and $E(A_1)$ are the vertical energies of the three excited states; κ_s and λ_s denote parameters of the LVC model referred to as *intrastate* and *interstate* coupling constants, respectively. The summations run over the normal (vibrational) modes of the specified symmetry. Q_s denote the (dimensionless) normal coordinates of the electronic ground state.[64–66] H_o is the vibrational Hamiltonian of the electronic ground state,

$$H_o=\frac{1}{2}\sum_{\substack{s\in a_1,\\ b_1,b_2}}\omega_s\left(-\frac{\partial^2}{\partial Q_s^2}+Q_s^2-1\right) \tag{2}$$

corresponding to noninteracting harmonic oscillators with frequencies ω_s. The vibrational ground state energy is taken as the origin of the energy scale. The quantities E, κ_s, λ_s, and ω_s represent parameters of the model, which can be determined, e.g., from the *ab initio* results for the adiabatic PES of the ground and excited electronic states. A detailed discussion of the parameterization procedure can be found in Refs. 28 and 29.

The coupling parameters determined from our EOM-CCSD results are listed in Table X. The present model does not take into account the hydrogen modes, as their contribution usually is small. Let us note that certain parameters reported here have to be viewed as preliminary, since they may not be accurate enough to qualify for the use in the dynamical calculations.[42] Table X shows also the κ_s constants for the states $^1B_1(3p)$ and $^1A_2(3p)$, which do not enter the above model. The vibrational excitation in the latter states will be described by independent Hamiltonians of the form,

B. Intersection of the S_1 and S_2 surfaces

The $B_2\times b_2$ instability predicted by our calculations and the low-lying intersection of the $S_1(^1B_2)$ and $S_2(^1A_2)$ states can be discussed by considering the (linear) vibronic coupling (LVC) systems, $^1B_2\times b_2\times{}^1A_1$ and $^1A_2\times b_1\times{}^1B_2$, respectively, which, of course, are not independent of each other. Let us analyze that situation in more detail using a suitable vibronic model Hamiltonian formulated for diabatic electronic states.[28,29] A LVC Hamiltonian describing both vibronic coupling problems in a unified way can be specified (using atomic units) as follows:

$$\mathbf{H}=H_o\mathbf{1}+E+\sum_{s\in a_1}\kappa_s Q_s. \tag{3}$$

The largest κ_s constants in all states are those for the modes ν_3 and ν_4, whereas the activity of the other a_1 modes is more state-specific. The strongest coupling arises from the modes ν_{19}, ν_{17} (b_2 in-plane vibrations, modifying the C–O bonds) and ν_{14} (b_1 out-of-plane vibration, simultaneously displacing the C_2 atoms with respect to both C_3 and O).

Having set up our model, we may proceed to the analysis of the adiabatic potential energy surfaces given by eigenvalues of the potential energy part of the Hamiltonians [Eqs. (1) and (3)]. Let us first consider the $B_2\times b_2$ instability. It arises due to the coupling of the $^1B_2(V)$ state and the $^1A_1(V')$ state. The cut through the PES along the ν_6 (a_1) mode shown in Fig. 4(A) visualizes the conical intersection of the $^1A_1(V')$ and $^1B_2(V)$ states as a crossing of the two curves. According to our model the minimal energy of this intersection (Table XI) is about 6.38 eV, that is, nearly the energy of the C_{2v} saddle point of the $^1A_1(V')$ state (6.36 eV). The cut through the PES in Fig. 5 along an effective coordinate, chosen as a combination of the b_2 coupling modes, demonstrates the effect of the coupling for the $^1A_1(V')$ and $^1B_2(V)$ states. One sees the typical double-well potential in the lower ($^1B_2$) state and a steeper shape of the potential in the upper ($^1A_1$) state, resulting from the repulsion of these states along the b_2 coordinate. Although the present results for the $^1A_1(V')$ state may be somewhat less accurate than for the other states (see Sec. III G), the qualitative picture given here should not be affected as long as the ordering of the $^1A_1(V')$ and $^1B_2(V)$ states does not change.

Another interesting feature in Fig. 5 is the intersection of

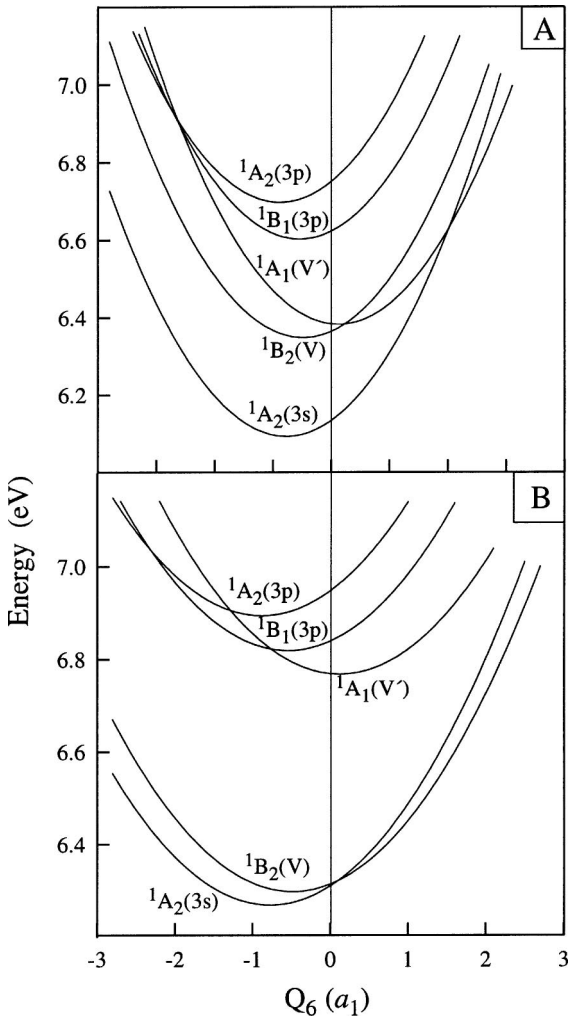

FIG. 4. LVC model potential energy curves for the normal coordinate Q_6 (a_1). The other totally-symmetric normal coordinates are set to: (A) values corresponding to the minimum energy of the conical intersection of the $^1A_1(V')$ and $^1B_2(V)$ states; (B) values corresponding to the minimum energy of the conical intersection of the $^1A_2(3s)$ and $^1B_2(V)$ states.

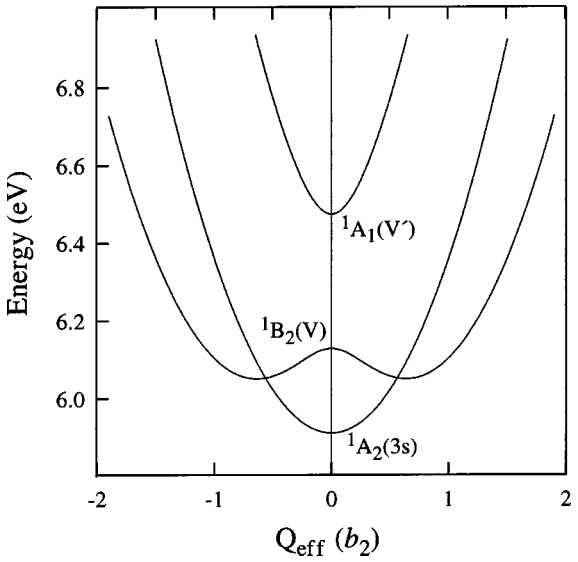

FIG. 5. Cut through the PES along an effective coordinate, chosen as a combination of the b_2 coupling modes. The double-well potential in the lower $^1B_2(V)$ state arises as a result of the interaction with the upper $^1A_1(V')$ state. The totally-symmetric normal coordinates are set to values corresponding to the equilibrium geometry of the $^1A'(V)$ state (C_s structure).

the $^1B_2(V)$ and $^1A_2(3s)$ states. The $^1A_2(3s)$ state, which cannot interact with the $^1A_1(V')$ and $^1B_2(V)$ states along the b_2 coordinate, is represented by a normal "unperturbed" potential curve. Obviously, its crossing with the $^1B_2(V)$ state becomes possible by the reshaping of the $^1B_2(V)$ curve as a result of the interaction with the $^1A_1(V')$ state.

The $^1B_2$–$^1A_2$ curve crossing seen in Fig. 5 obviously is associated with a conical intersection of these states. This intersection is, however, unusual, since it involves nontotally symmetric b_2 modes acting as additional "tuning" modes.

TABLE XI. Minimal energy of conical intersections (eV) between various low-lying excited singlet states of furan, as predicted by the linear vibronic model.[a]

	$^1B_2$ (V)	$^1B_1$ $(3p)$	$^1A_1$ (V')	$^1A_2$ $(3p)$
$^1A_2$ $(3s)$	6.32	>10	6.47	>10
$^1B_2$ (V)		6.54	6.38	6.99
$^1B_1$ $(3p)$			6.42	6.78
$^1A_1$ (V')				6.51

[a]See text for details.

Cuts through the PES along one of the (a_1) tuning modes are shown in Fig. 4(B). Here the $^1B_2$–$^1A_2$ intersection can be seen as a curve crossing at an energy of about 6.32 eV, that is, well above the energy of the C_{2v} structure of the $^1B_2(V)$ state (6.11 eV). Returning to the situation in Fig. 5, one sees that in this case the intersection of the $^1B_2$–$^1A_2$ states lies only slightly higher than the bottom of the $^1A'(V)$ state (6.07 eV) and below the C_{2v} structure of the $^1B_2(V)$ state. The additional lowering of the energy of the intersection is due to role of the b_2 modes in the tuning of the conical intersection point.

A possible coupling coordinate for the $^1B_2$–$^1A_2$ interaction must be of b_1 symmetry. As has been mentioned above, the coupling along these modes has only moderate strength, so that no strong effect can be expected. Two cuts through the PES along the Q_{14} (b_1) coordinate are shown in Figs. 6(A) and 6(B), respectively. The cut in Fig. 6(B) demonstrates that at the minimum of the $^1A_2$ state the lowest PES is flattened by the interaction, but retains a single-well shape. The situation is different at the point of the $^1A'(V)$ state (C_s stationary point of S_1), which "feels" the presence of the closely located intersection [Fig. 6(A)]. Here, the lower potential develops a double minimum, making the $^1A'(V)$ state unstable with respect to a distortion along the b_1 coordinate. That effect has, however, only local character and disappears as soon as one goes away from the intersection point. In Fig. 7 the situation is visualized by three-dimensional views of the S_1 and S_2 surfaces plotted as a function of the b_1 (out-of-plane bending) and b_2 (in-plane bending) coordinates.

The plots in Fig. 7 are also quite instructive for the description of the processes following the vertical excitation to the $^1B_2(V)$ state. Starting at the C_{2v} saddle point of the $^1B_2(V)$ state the system will begin to relax along the b_2 coordinate. Since this coordinate does not mix $^1B_2(V)$ and

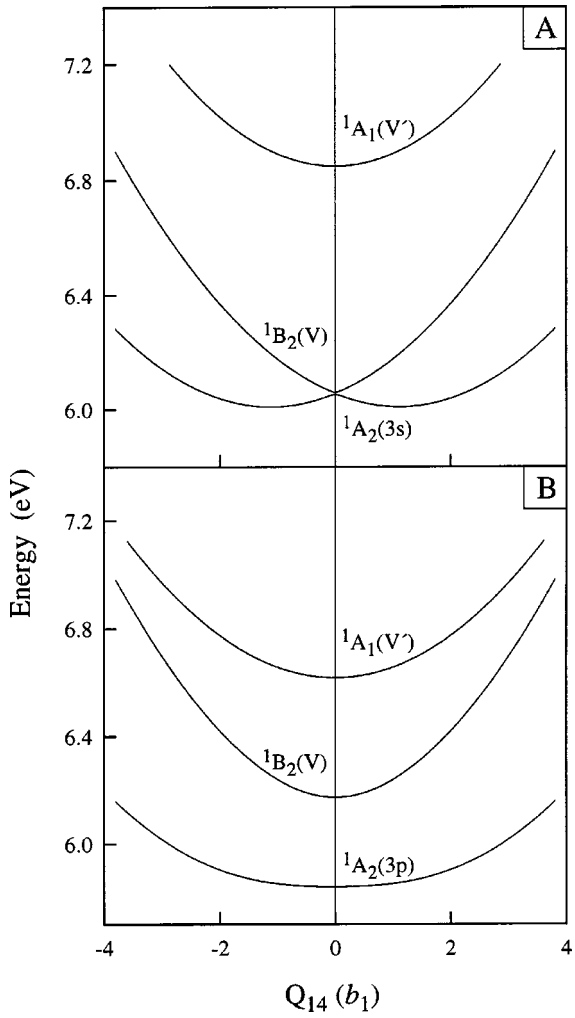

FIG. 6. LVC model potential energy curves for the normal coordinate Q_{14} (b_1). The other normal coordinates are set to: (A) values corresponding to the equilibrium geometry of the $^1A'(V)$ state (C_s structure); (B) values corresponding to the equilibrium geometry of the $^1A_2(3s)$ state (C_{2v} structure).

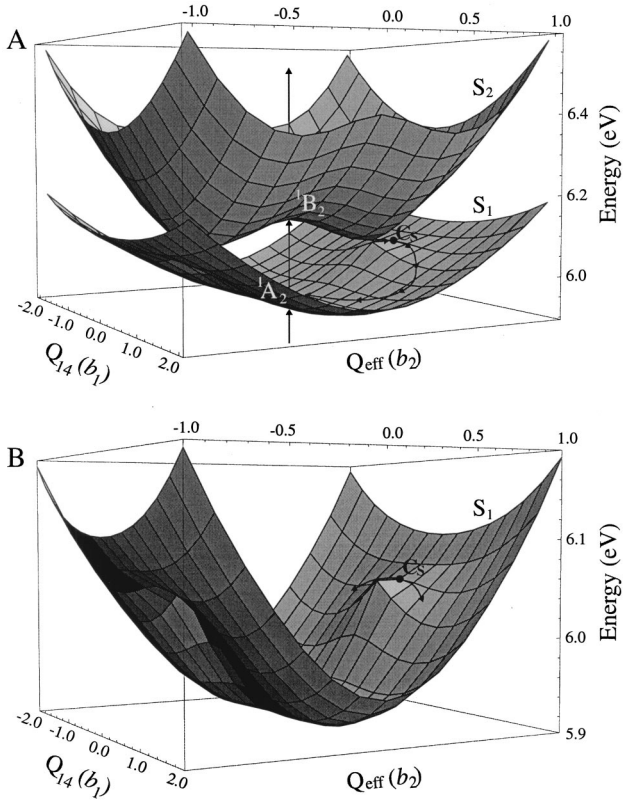

FIG. 7. Three dimensional (3D) view of the S_1 and S_2 PES (A) and S_1 PES (B) with respect to the effective coordinate, chosen as a combination of the b_2 modes, and the normal coordinate Q_{14} (b_1). The other normal coordinates are set to values corresponding to the equilibrium geometry of the $^1A'(V)$ state (C_s structure).

$^1A_2(3s)$ states, the relaxation path crosses the conical intersection point and reaches the $^1A'(V)$ state (which is a C_s saddle point of S_1). Since the latter structure itself is unstable with respect to the b_1 coordinate, the relaxation will proceed further on the S_1 surface, bringing the system from the C_s structure down to a "valley," and then along the valley to the bottom (C_{2v} minimum) of the S_1 surface, that is, to the $^1A_2(3s)$ state. Using a geometrical language this can be also described as follows (see Fig. 8): Upon vertical excitation to the $^1B_2(V)$ state of the (upper) S_2 surface, furan distorts to the planar C_s structure, and then, via a (small) out-of-plane deformation, returns to symmetric C_{2v} configuration associated with the $^1A_2(3s)$ state of the (lower) S_1 surface.

C. Other vibronic interactions

In the preceding section we have analyzed the $^1B_2\times b_2\times{}^1A_1$ and $^1A_2\times b_1\times{}^1B_2$ vibronic coupling mechanisms, which influence most strongly the structure and dynamics of the S_1 and S_2 states. These two mechanisms should clearly constitute the backbone of any vibronic coupling model for studying the excited-state nuclear dynamics in furan. There are, however, further interactions, which could be important for the excitation spectrum of furan and possibly should be considered in a model for dynamical studies.

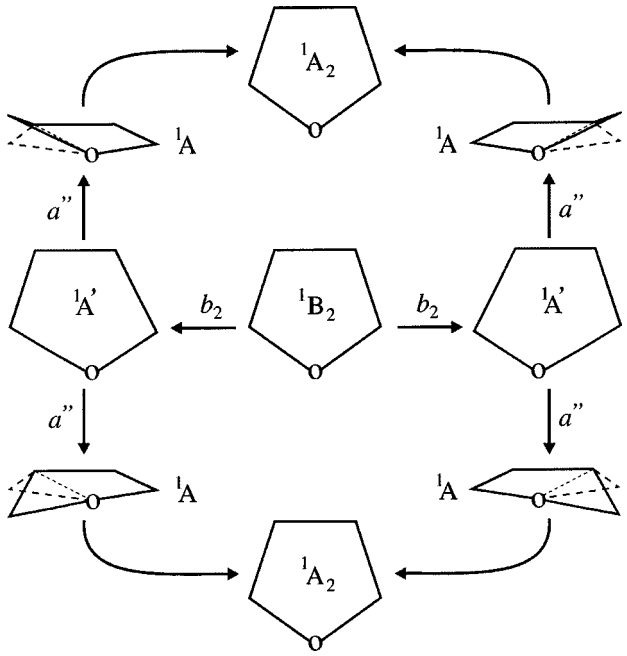

FIG. 8. Schematic description of the relaxation process taking place in furan upon excitation to the $^1B_2(V)$ state.

The cuts along the totally-symmetric modes in Figs. 4(A) and 4(B) show additional curve crossings for the following pairs of states: $^1A_2(3s)$ and $^1A_1(V')$, $^1B_2(V)$ and $^1B_1(3p)$, $^1A_1(V')$ and $^1B_1(3p)$, $^1A_1(V')$ and $^1A_2(3p)$, $^1B_1(3p)$ and $^1A_2(3p)$. All these crossings are related to conical intersections associated with individual vibronic coupling schemes (see also Table XI).

As has been noticed in Sec. III C, the $^1A_2(3s)$ PES is flattened along certain b_1, b_2, and a_2 modes (the vibrational frequencies of these modes being appreciably reduced as compared to the ground state). Speaking in terms of linear vibronic couplings, this may indicate interactions with higher-lying states of $^1B_2$, $^1B_1$, and $^1A_1$ symmetry. The interaction with the $^1B_2(V)$ valence state was already considered above. The interaction with the $^1B_1$ state, having an appreciable optical transition strength, might be important for the modeling of the absorption spectrum, since it can lead to a transfer of spectral intensity to the dipole-forbidden $^1A_2(3s)$ transition (intensity borrowing effect). The interaction with the $^1A_1(V')$ state will be less relevant here due to the extremely small optical strength of the $V'(^1A_1)$ transition.

A reduction of the vibrational frequencies has been noticed also for some b_1 and a_2 modes in the $^1B_2(V)$ state (Sec. III D). This suggests vibronic coupling of the $^1B_2(V)$ state to some higher-lying $^1A_2$ and $^1B_1$ states.

The vibrational frequencies found for the $^1B_1(3p)$ state are quite similar to those seen in the electronic ground state, which could be interpreted as an indication that the $^1B_1(3p)$ state is not involved in the vibronic couplings to the other states. On the other hand, we have seen above that there are at least two conical intersections involving the $^1B_1(3p)$ state, and, moreover, we have argued that there should be an interaction with the $^1B_2(V)$ state. Let us recall that our simple considerations were based on a two-state vibronic coupling model, which may not apply to the case, where a state is coupled to states lying above and below it by modes of one symmetry. Here the two couplings have opposite effects and the actual shape of the PES will be determined by the balance between them. For the $^1B_1(3p)$ state this means that the influence of the lower-lying $^1B_2(V)$ state may be compensated by the interaction with higher-lying states of $^1B_2$ symmetry, so that we do not see any change of the vibrational frequencies of the coupling a_2 modes here. Such a situation may represent a difficulty for LVC models, since it requires to introduce higher-lying states, even when these are of no interest of their own.

The vibronic coupling schemes addressed so far do not explain the structural instabilities of the $^1A_1(V')$ state with respect to b_1 and b_2 distortions. Clearly, these could be taken into account by the interaction of the $^1A_1(V')$ state with higher-lying $^1B_1$ and $^1B_2$ states.

D. Spectroscopic implications

As we have seen, all of the low-lying excited singlet states of furan are entangled by vibronic coupling and a multitude of conical intersections connects their potential energy surfaces. One has to expect that this intricate situation will be reflected by a very complex excitation spectrum.

Strong nonadiabatic effects can be expected in the excitation spectrum above the lowest conical intersection of the S_1 and S_2 PES, taking place at about 6 eV. As is well known,[28,29] above a conical intersection the nuclear dynamics no longer proceeds on the individual PES. An adiabatic description of the excitation applies only to the very lowest part of the spectrum, that is, the energy region around 5.8–6.0 eV. Here, the present calculations predict only vibrational levels of the $^1A_2(3s)$ state, which is dipole-forbidden. Via intensity borrowing induced by vibronic coupling, here with the $^1B_2(V)$ and $^1B_1(3p)$ states, certain vibrational levels of the $^1A_2(3s)$ state will acquire spectral intensity. These $^1A_2(3s)$ transitions seem to be attributable to the shoulders on the low-energy side of the first band in the experimental VUV spectrum of furan, beginning at about 5.7 eV.

The second state in the spectrum, $^1B_2(V)$, is strongly affected by the interaction with the lower- and higher-lying $^1A_2(3s)$ and $^1A_1(V')$ states, respectively. As a result of these interactions, the $^1B_2(V)$ state can be considered as ''unbound'' with respect to coordinates of b_2 symmetry; along these coordinates the symmetric molecular configuration is unstable and a relaxation process takes the system through the conical intersection of the S_1 and S_2 surfaces to the lower surface, proceeding further until the minimum of the $^1A_2(3s)$ state. This relaxation path represents a very fast internal conversion channel from the $^1B_2(V)$ to the $^1A_2(3s)$ state. A number of other internal-conversion processes from higher-lying singlet excited states to the $^1A_2(3s)$ state can be expected. Such relaxation mechanisms may partly explain the highly diffuse character of the experimental VUV spectrum and the previous difficulties with its assignment.

In view of the complex spectral situation we must refrain in this work from trying to assign the experimental features on the basis of the present vertical and adiabatic results (Tables I and VII). What is required for that purpose is a rigorous treatment of the nuclear dynamics for the system of coupled surfaces. Such a study, based on the vibronic coupling model established in the present work and carried out using large-scale wave-packet propagation techniques, is under way,[42] and we may postpone the interpretation of the excitation spectrum until the results of that study will be available.

V. SUMMARY AND CONCLUSIONS

In the present work we have studied in some detail the manifold of low-lying excited singlet states of furan, comprising (at the equilibrium ground-state C_{2v} molecular configuration) the lowest two $^1A_2(3s)$ and $^1B_1(3p)$ Rydberg states and the two $^1B_2(V)$ and $^1A_1(V')$ valence states.

Extensive *ab initio* electronic structure calculations have been carried out using the equation-of-motion coupled-cluster singles and doubles method (EOM-CCSD).[38] A study of the vertical excitations energies has been performed, which confirmed that the employed method and basis set are capable of providing an accuracy of about 0.2 eV, which is sufficient for a reliable description of the excitation spectrum.

TABLE XII. Total and zero-point vibrational (ZPVE) energies (Hartree) for the ground and low-lying excited singlet states of furan at different geometries of the molecule.

Geometry	Symmetry	Type	$\tilde{X}\,^1A_1$[a]	$^1A_2\,(3s)$[a]	$^1B_2\,(V)$[a]	$^1B_1\,(3p)$[a]	$^1A_1\,(V')$[a]	$^1A_2\,(3p)$[a]	ZPVE
$\tilde{X}\,^1A_1$	C_{2v}	min	−229.427296	−229.206267	−229.190702	−229.187340	−229.180312	−229.181418	0.070122
Expt.[b]	C_{2v}		−229.426233	−229.205514	−229.188929	−229.186072	−229.175957	−229.180636	
$^1A_2\,(3s)$	C_{2v}	min	−229.421147	−229.212666	−229.200137	−229.192950	−229.184080		0.068307
$^1B_2\,(V)$	C_{2v}	saddle	−229.414864	−229.209354	−229.202902	−229.189949	−229.186191		0.062880
$^1A'\,(V)$	C_s	saddle	−229.407718	−229.203655	−229.204086	−229.184424	−229.176799		0.062031
$^1B_1\,(3p)$	C_{2v}	min	−229.421511	−229.212490	−229.200246	−229.193126	−229.185513		0.068975
$^1A_1\,(V')$	C_{2v}	saddle	−229.413580	−229.202905	−229.195592	−229.184941	−229.193430		
$^1A'\,(V')$	C_s	?	−229.403548	−229.195397	−229.185384	−229.170044	−229.194340		
$^1A\,(V')$	C_2	?	−229.405925	−229.195249	−229.192525	−229.176441	−229.194240		

[a]Designation of PES at the C_{2v} configuration.
[b]Experimental ground state geometry (Ref. 50).

Particular emphasis has been put on the exploration of the adiabatic potential energy surfaces in the vicinity of the ground-state equilibrium geometry. Using the analytical gradient techniques available in the EOM-CCSD approach,[41] we have performed full geometry optimizations for the most important stationary points on the PES of the low-lying excited singlet states. The located stationary points have been characterized by harmonic vibrational analysis.

The major new result of this work is that the $^1B_2(V)$ valence state is unstable with respect to non-totally symmetric distortions at the C_{2v} configuration. The symmetry breaking involves an in-plane vibrational coordinate of b_2 symmetry, which leads to a planar C_s structure [$^1A'(V)$ state] with nonequivalent bonds and angles. This is a new type of symmetry breaking, not previously known to occur in five-membered aromatic ring molecules. An interesting feature of the discovered relaxation process is that it begins at the symmetric molecular configuration of the S_2 PES [$^1B_2(V)$ state], then passes through a low-lying conical intersection of the S_1 and S_2 PES, and continues on the lower (S_1) surface. The latter part of the process comprises a step, in which a planar C_s structure [$^1A'(V)$ state] is reached, and a further step, in which the C_s structure undergoes an out-of-plane (a'') symmetry breaking, finally taking the system to the adiabatic minimum of the S_1 PES [$^1A_2(3s)$ state]. The $^1B_2(V)$ state can therefore be considered as ''unbound'' with respect to the b_2 coordinate, its relaxation cycle representing a channel for a fast internal conversion to the lower-lying $^1A_2(3s)$ state.

Another important finding of the present work concerns the $^1A_1(V')$ valence state, which was predicted to be unstable with respect to b_1 and a_2 out-of-plane bending coordinates, leading to structures of C_s and C_2 symmetry, respectively. Though most of the distorted excited-state structures identified in the present work are characterized by very small stabilization energies (and therefore may not be individually observable states), they should certainly be very important for the understanding of the spectroscopy and photochemistry of furan and related heterocyclic molecules.

The vibronic mechanism that couples the S_1 and S_2 adiabatic PES has been analyzed in detail using a linear vibronic coupling model, involving the coupled interactions $^1B_2\times b_2\times{}^1A_1$ and $^1A_2\times b_1\times{}^1B_2$. These interactions are the key to an understanding of singlet excited-state nuclear dynamics of furan at lower energy. It has been shown that there are other interactions, which might become important in the modeling of the vibronic spectrum. We have detected a multitude of conical intersections involving the low-lying singlet excited states, indicating that one has to expect extensive vibronic coupling.

Our findings elucidate the great complexity of the observed excitation spectrum and explain previous difficulties of making assignments. We predict that the singlet excitation of furan proceeds predominantly in a truly nonadiabatic regime, beginning at about 6 eV. Below this energy only a few distinct vibrational levels of the $^1A_2(3s)$ state are to be expected, which acquire their spectral intensity from the upper-lying dipole allowed $V(^1B_2)$ and $3p(^1B_1)$ transitions via an intensity borrowing mechanism.

The present work sets up the basis and the background for an ensuing wave-packet dynamical study of the furan excitation spectrum, which we hope to present in the near future.[42]

ACKNOWLEDGMENTS

This work has been supported by the *Russian Foundation for Basic Research* (RFBR) and by the *Deutsche Forschungsgemeinschaft* (DFG). Two of the authors (E.V.G. and A.B.T.) are grateful for the hospitality and support experienced during their stays at the Heidelberg Theoretical Chemistry Group. The authors are indebted to L. S. Cederbaum for his interest in this work and for valuable discussions.

APPENDIX: LIST OF TOTAL ENERGIES FOR ALL STATES AT VARIOUS NUCLEAR CONFORMATIONS

In Table XII we list the total ground- and excited-state energies obtained for various molecular structures of furan considered in this work. In the cases, where a full harmonic vibrational analysis could be performed, also the zero-point vibrational energy (ZPVE) are given. The results summarized in Table XII should allow one to deduce all excitation energies and energy differences discussed in the paper (to obtain the energy values in eV we used the conversion factor 1 Hartree = 27.211 606 eV).

[1] *The Chemistry of Heterocyclic Compounds*, edited by R.A. Jones, E.C. Taylor, and A. Weissberger (Wiley, New York, 1990), Vol. 48, Part I; *ibid.*, Part 2 (Wiley, New York, 1992); *Conjugated Polymers: The Novel Science and Technology of Highly Conducting and Nonlinear Optically Active Materials*, edited by J.L. Brédas and R. Silbey (Kluwer, Dordrecht, 1991).
[2] O. Sorkhabi, F. Qi, A.H. Rizvi, and A.G. Suits, J. Chem. Phys. **111**, 100 (1999).
[3] M.H. Palmer, I.C. Walker, C.C Ballard, and M.F. Guest, Chem. Phys. **192**, 111 (1995).
[4] L. Nyulászi, J. Mol. Struct. **273**, 133 (1992).
[5] M.B. Robin, *Higher Excited States of Polyatomic Molecules* (Academic, New York, 1975), Vol. 2; *ibid.* (Academic, New York, 1985), Vol. 3.
[6] J.L. Roebber, D.P. Gerrity, R. Hemley, and V. Vaida, Chem. Phys. Lett. **75**, 104 (1980).
[7] C.D. Cooper, A.D. Williamson, J.C. Miller, and R.N. Compton, J. Chem. Phys. **73**, 1527 (1980).
[8] L. Sanche, J. Chem. Phys. **71**, 4860 (1979).
[9] B. Nordén, R. Håkansson, P.B. Pedersen, and E.W. Thulstrup, Chem. Phys. **33**, 355 (1978).
[10] E.H. van Veen, Chem. Phys. Lett. **41**, 535 (1976).
[11] W.M. Flicker, O.A. Mosher, and A. Kuppermann, Chem. Phys. Lett. **38**, 489 (1976); J. Chem. Phys. **64**, 1315 (1976).
[12] P.J. Derrick, L. Åsbrink, O. Edqvist, B.Ö. Jonsson, and E. Lindholm, Int. J. Mass Spectrom. Ion Phys. **6**, 161 (1971).
[13] G. Horvath and A.I. Kiss, Spectrochim. Acta, Part A **23A**, 921 (1967).
[14] K. Watanabe and T. Nakayama, J. Chem. Phys. **29**, 48 (1958).
[15] L.W. Pickett, N.J. Hoeflich, and T.-C. Liu, J. Am. Chem. Soc. **73**, 4865 (1951).
[16] W.C. Price and A.D. Walsh, Proc. R. Soc. London, Ser. A **179**, 201 (1941).
[17] L.W. Picket, J. Chem. Phys. **8**, 293 (1940).
[18] R. Burcl, R.D. Amos, and N.C. Handy, Chem. Phys. Lett. **355**, 8 (2002).
[19] J. Wan, J. Meller, M. Hada, M. Ehara, and H. Nakatsuji, J. Chem. Phys. **113**, 7853 (2000).
[20] M. D'Auria, J. Org. Chem. **65**, 2494 (2000).
[21] O. Christiansen and P. Jørgensen, J. Am. Chem. Soc. **120**, 3423 (1998).
[22] O. Christiansen, A. Halkier, H. Koch, and P. Jørgensen, J. Chem. Phys. **108**, 2801 (1998).
[23] A.B. Trofimov and J. Schirmer, Chem. Phys. **224**, 175 (1997).
[24] H. Nakano, T. Tsuneda, T. Hashimoto, and K. Hirao, J. Chem. Phys. **104**, 2312 (1996).
[25] L. Serrano-Andrés, M. Merchán, I. Nebot-Gil, B.O. Roos, and M. Fülscher, J. Am. Chem. Soc. **115**, 6184 (1993).
[26] H. Nakatsuji, O. Kitao, and T. Yonezawa, J. Chem. Phys. **83**, 723 (1985).
[27] K.-H. Thunemann, R.J. Buenker, and W. Butscher, Chem. Phys. **47**, 313 (1980).
[28] H. Köppel, W. Domcke, and L.S. Cederbaum, Adv. Chem. Phys. **57**, 59 (1984).
[29] H. Köppel and W. Domcke, in *Encyclopedia in Computational Chemistry*, edited by P. von Ragué (Wiley, New York, 1998), p. 3166.
[30] W. Domcke and G. Stock, Adv. Chem. Phys. **100**, 1 (1997).
[31] D.R. Yarkony, J. Phys. Chem. **100**, 18612 (1996).
[32] I.B. Bersuker, Chem. Rev. **101**, 1067 (2001).
[33] P.V. Schastnev and L.N. Shchegoleva, *Molecular Distortions in Ionic and Excited States* (CRC, Boca Raton, 1995), pp. 79–81.
[34] A.B. Trofimov, H. Köppel, and J. Schirmer, J. Chem. Phys. **109**, 1025 (1998).
[35] G. Herzberg and H.C. Longuet-Higgins, Discuss. Faraday Soc. **35**, 77 (1963); T. Carrington, *ibid.* **53**, 27 (1972); H.C. Longuet-Higgins, U. Öpik, M.H. Pryce, and R.A. Sack, Proc. R. Soc. London, Ser. A **244**, 1 (1958).
[36] D.R. Yarkony, J. Phys. Chem. A **105**, 6277 (2001); Rev. Mod. Phys. **68**, 985 (1996).
[37] O. Christiansen, H. Koch, and P. Jørgensen, Chem. Phys. Lett. **243**, 409 (1995).
[38] H. Sekino and R. J. Bartlett, Int. J. Quantum Chem., Quantum Chem. Symp. **18**, 255 (1984); J. Geertsen, M. Rittby, and R. J. Bartlett, Chem. Phys. Lett. **164**, 57 (1989); J.F. Stanton and R.J. Bartlett, J. Chem. Phys. **98**, 7029 (1993).
[39] H. Nakatsuji and K. Hirao, Chem. Phys. Lett. **47**, 569 (1977); H. Nakatsuji, *ibid.* **67**, 329 (1979); **67**, 334 (1979).
[40] E. Dalgaard and H.J. Monkhorst, Phys. Rev. A **28**, 1217 (1983); H. Koch and P. Jørgensen, J. Chem. Phys. **93**, 3333 (1990); H. Koch, H. J. A. Jensen, P. Jørgensen, and T. Helgaker, *ibid.* **93**, 3345 (1990).
[41] J.F. Stanton, J. Chem. Phys. **99**, 8840 (1993).
[42] E.V. Gromov, A.B. Trofimov, N.M. Vitkovskaya, J. Schirmer, H. Köppel, H.-D. Meyer, and L.S. Cederbaum (unpublished).
[43] ACES II is a program product of the Quantum Theory Project, University of Florida, J.F. Stanton, J. Gauss, J.D. Watts *et al.*, Integral packages included are VMOL (J. Almlöf and P.R. Taylor); VPROPS (P. Taylor); ABACUS (T. Helgaker, H.J. Aa. Jensen, P. Jørgensen, J. Olsen, and P.R. Taylor).
[44] G.D. Purvis and R.J. Bartlett, J. Chem. Phys. **76**, 1910 (1982).
[45] H.-J. Werner and P.J. Knowles, J. Chem. Phys. **89**, 5803 (1988); P.J. Knowles and H.-J. Werner, Chem. Phys. Lett. **145**, 514 (1988).
[46] H.-J. Werner and P.J. Knowles, J. Chem. Phys. **82**, 5053 (1985); P.J. Knowles and H.-J. Werner, Chem. Phys. Lett. **115**, 259 (1985).
[47] MOLPRO, a package of *ab initio* programs designed by H.-J. Werner and P. J. Knowles, *et al.*, version 2002.1.
[48] T.H. Dunning, Jr., J. Chem. Phys. **90**, 1007 (1989).
[49] R.A. Kendall, T.H. Dunning, Jr., and R.J. Harrison, J. Chem. Phys. **96**, 6796 (1992).
[50] F. Mata, M.C. Martin, and G.O. Sørensen, J. Mol. Struct. **48**, 157 (1978).
[51] E. Larsen, K. Hald, J. Olsen, and P. Jørgensen, J. Chem. Phys. **115**, 3015 (2001); K. Hald, C. Hättig, J. Olsen, and P. Jørgensen, *ibid.* **115**, 3545 (2001); O. Christiansen, H. Koch, P. Jørgensen, and J. Olsen, Chem. Phys. Lett. **256**, 185 (1996); H. Koch, O. Christiansen, P. Jørgensen, and J. Olsen, *ibid.* **244**, 75 (1995).
[52] A.B. Trofimov, G. Stelter, and J. Schirmer, J. Chem. Phys. **117**, 6402 (2002).
[53] A.B. Trofimov, G. Stelter, and J. Schirmer, J. Chem. Phys. **111**, 9982 (1999).
[54] L. Nygaard, J.T. Nielsen, J. Kirchheimer, G. Maltesen, N. Rastrup-Andersen, and G.O. Sorensen, J. Mol. Struct. **3**, 491 (1969).
[55] A. Mellouki, J. Liévin, and M. Herman, Chem. Phys. **271**, 239 (2001).
[56] M. Rico, M. Barrachina, and J.M. Orza, J. Mol. Spectrosc. **24**, 133 (1967).
[57] R.C. Lord, Jr. and F.A. Miller, J. Chem. Phys. **10**, 328 (1942).
[58] When comparing harmonic frequencies of the different electronic states one should be aware that the two sets of normal modes can often be quite distinct.
[59] The absence of a structural instability (symmetry breaking) in the $^1B_2(V)$ state follows from the results of Table II in Ref. 21.
[60] B. O. Roos, P.-Å. Malmqvist, and V. Molina, J. Chem. Phys. **116**, 7526 (2002).
[61] In certain cases the calculations converge to a wrong root ("root flipping" problem), which is probably related to fact that the CIS scheme is used for the construction of a trial vector in the iterative solution of the EOM-CCSD equations. Since the CIS does not account for doubly-excited configurations, the resulting trial vectors may poorly describe the state under investigation.
[62] F. Negri and Z. Zgierski, J. Chem. Phys. **100**, 2571 (1994).
[63] Z. Zgierski and F. Zerbetto, J. Chem. Phys. **99**, 3721 (1993).
[64] The dimensionless normal coordinates Q_s used in the present work are obtained from those of Wilson *et al.* (Ref. 62) by multiplying with $\sqrt{\omega_s}$ (where ω_s is the ground-state vibrational frequency for mode ν_s).
[65] E.B. Wilson, Jr., J.C. Decius, and P.C. Cross, *Molecular Vibrations* (McGraw–Hill, New York 1955).
[66] L.S. Cederbaum and W. Domcke, Adv. Chem. Phys. **36**, 205 (1977).